Comparative study of the effect of several trains on the rotation motion of ballast stones

Fermín Navarro-Medina, Isabel Perez-Grande, Angel Sanz-Andres

Abstract

The ballast pick-up (or ballast train-induced-wind erosion (BTE)) phenomenon is a limiting factor for the maximum allowed operational train speed. The determination of the conditions for the initiation of the motion of the ballast stones due to the wind gust created by high-speed trains is critical to predict the start of ballast pick-up because, once the motion is initiated, a saltation-like chain reaction can take place. The aim of this paper is to present a model to evaluate the effect of a random aerodynamic impulse on stone motion initiation, and an experimental study performed to check the capability of the proposed model to classify trains by their effect on the ballast due to the flow generated by the trains. A measurement study has been performed at kp 69+500 on the Madrid – Barcelona High Speed Line. The obtained results show the feasibility of the proposed method, and contribute to a technique for BTE characterization, which can be relevant for the development of train interoperability standards.

Introduction

Ballast pick-up is a problem that has recently appeared on high-speed train lines as a result of increased train operating speeds. In addition to damage to the train, the railhead can also be affected by ballast pitting.[1] These problems may become critical and can result in a speed limit being put into operation. This limit would reduce the maximum transport capacity of the line, and therefore, the determination of the effect on the ballast of the flow generated by a train is receiving considerable attention from research institutions in the rail transportation field. Generally speaking, this effect can be split into two complementary parts: one is the wind capacity acting on the trackbed, or 'ballast train-induced-wind erosion' (BTE); and the other is the erodibility or erosibility,[2] which is the capacity of the soil (or trackbed) to resist the mechanical action of the wind, it depends on the soil particle size and distribution, density, agglomeration, etc.

To investigate the BTE capacity of a given train and compare it with others, local random characteristics of the ballast (mass, posture, size, surroundings) can be neglected in a first approach). However, these local characteristics can be associated with ballast erodibility. A statistical approach to these random aspects can be found in Sanz-Andres and Navarro-Medina.[3]

The aim of this paper is to help to develop standard procedures that allow for the definition (by railway authorities) of tests aimed at determining the BTE effect created by new trains.

There is not much published work concerning the problem of flying ballast, in spite of the great interest that exists due to its relevance in increasing the maximum operative train speed. The initiation of the flight of ballast due to the passing of a high-speed train has

been studied by Kwon and Park,[4] who performed experiments in a wind tunnel and in the field. They obtained probabilistic results for flying ballast stones, but did not considered the mechanisms that initiated the motion, which are important at the phase of the BTE process studied in this paper.

The velocity field under a train has been studied by Sterling et al.[5] and Baker[6] among others. Their research was focused on the description of the velocity field between the train's underbody and the trackbed, which can be useful to study the trajectory of the ballast once it has taken-off. However, the force on the ballast is the essential variable that needs be known to study the initiation of the motion, instead of considering the wind speed.

Due to the unsteadiness of the flow, the pressure field acting on the stones is dependent not only on the speed itself but also on the time derivative so that a proportional relationship between the pressure field and the dynamic pressure (or velocity pressure) cannot be directly applied.

Concerning tests on operational tracks, there have been some measurement studies that have dealt with the effects on the infrastructure of the passing of trains, e.g. Quinn et al.,[1] but most of the results obtained in these studies are commercially sensitive and are not available in the open literature. Also, these measurement studies have focused mainly on the velocity field generated close to the track by a train and not on the force acting on the ballast.

Quinn et al.[1] discussed the mechanism of initiation of the flight of ballast particles, which requires the ballast particles to acquire a vertical velocity component to start the flight, as has also been pointed out in some previous experiments concerning saltation processes of soil eolian erosion.[7–9] Before the initiation of flight, a roll-jump process of the ballast stones has been reported by Kwon and Park.[4] The initial rotation, together with the rolling-jumping phase, is an intermediate phase between the initial equilibrium and the final flight, a phase that is more relevant in the case of a time-varying, gusty flow, such as the one generated by the passage of a train. With regard to this intermediate phase, a new theoretical approach concerning the determination of the conditions for the initiation of the motion of the ballast stones due to the wind gust created under high-speed trains was recently developed by Sanz-Andres and Navarro-Medina.[3]

The initiation of motion occurs when the aerodynamic moment becomes greater than the stabilizing moment (generated by the force of gravity). Both moments are calculated with regard to the pivot point (point P in Figure 1)), which depends on the posture of the stone on the surrounding ballast. The initiation of the motion is successful when both the intensity and duration of the net moment are great enough to give the stone enough kinetic energy. In this case the stone starts to rotate and surpasses a limiting rotation angle or 'vertical position' (see Figure 1(c)). Beyond this position there is no return to its previous equilibrium position; otherwise, the stone falls back towards its original position (frustrated initiation).

Obviously, the intensity and duration of the net moment required for a successful motion of a given stone depend on a number of stone-related parameters, among others, the size, density and shape of the stone, and its posture on the trackbed.

In order to establish a parameter that measures the BTE ability, independent of both the ballast characteristics and of the way a stone moves during the initial rotation phase, this paper considers the angular impulse (in dimensionless form) which would be applied to a stone by the net moment once the threshold for motion is attained, that is, when the applied aerodynamic moment surpasses the stabilizing moment due to gravity. To allow for the comparison of the effects produced by different trains to be carried out, this angular impulse has to be measured on a suitably 'standardized' test body placed on the track, the same for all trains.

The aim of this study is to generate knowledge on methods to compare the effect on the ballast produced by different high-speed trains. As previously mentioned, the BTE effect on the ballast depends on the

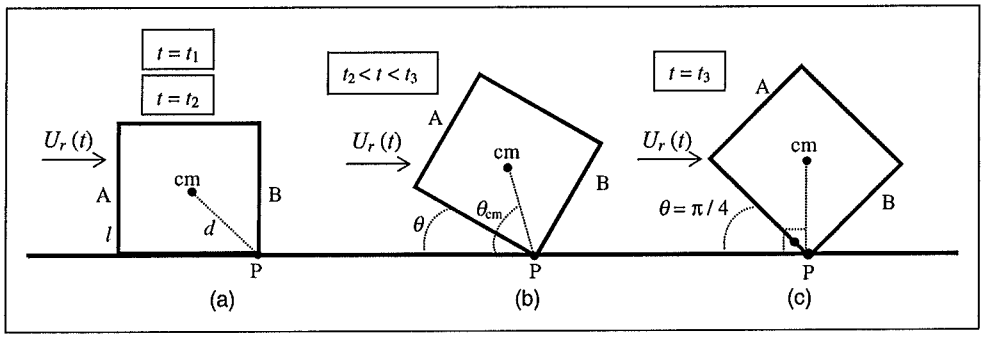

Figure 1. Sketch of the considered configuration. (a) The body is lying or remains close to the floor (b) it rotates around its trailing edge P and (c) it is at the stability limit with the centre of mass at the highest position. $U_r(t)$: wind speed; cm: centre of mass; θ: angular position of the body.

stone's shape, orientation and surrounding stones. Even if a measurement method could capture the influence of all these factors, the results would be random because of two sources:

- the ballast stone characteristics and orientation (erodibility);
- the turbulent flow generated by the train (BTE).

A preliminary analysis devoted to study the first type can be found in Sanz-Andres and Navarro-Medina.[3] If the aim is tocompare several trains, the test body should be the same for all of them, and its characteristics should be chosen in such a way that the random contribution due to erodibility can be eliminated. Thus, the body should easily and repeatedly be placed on the ballast track, and not be affected by the surrounding stones, while making possible the measurement of the wind effect at the ballast bed height. To accomplish these goals, a standard body with a height that is similar to the ballast stone's characteristic dimensions, placed on a plane surface (to avoid random shapes and orientations of surrounding stones), and with a two-dimensional shape (to avoid the complex flow generated by the measured body) is used. The effect of the wind generated by the train on this body is experimentally studied, and validated with a simple theoretical model.

The most direct measurement of the aerodynamic loads may appear to be the measurement of the force (or moment) on a stone-like body, but fitted with a load cell. However, this technique implies the use of delicate instrumentation due to the small size of the test body. Also, the measurements can be greatly perturbed by the effect of the inertial forces acting both on the test body and on the instrument support, due to the difficulty in isolating the base of the load cell from the vibrations of the track produced by the train passage.[1]

A simpler option, the one employed in the present paper, is to measure the aerodynamic load, that is, the pressure field that is generated on a suitable standard test body by the flow created by a train. Fortunately, the pressure measurements can be readily performed even at relatively high sampling rates, and pressure sensors are not significantly affected by track vibrations.

As previously mentioned, this pressure field cannot be readily obtained from the velocity field because Bernoulli's equation cannot be used without a careful consideration in advance of its applicability to this case, analysing the contribution of both rotational and non-steady effects. Additionally, the orientation of the pressure tap with regard to the incoming flow has a large influence on the measurement. These are some of the reasons why the comparison between pressure and velocity fields measurements obtained by Quinn et al.[1] (where the orientation of pressure taps is not described) is not possible.

In this paper the results of the performed measurements, together with a simple mathematical model that can help to analyse the results and a statistical study of their characteristics are presented. It is shown that the averaged histogram of the net impulse exerted on the model can help to classify the relative BTE capacity of the measured trains.

The performed experiments show that the trains can be identified in terms of a characteristic signature, which is related to the geometry of the train's underbody. Unfortunately, information about the train's underbody is not available because companies regard such information as being commercially sensitive. However, in order to explain the effect of the lower part of the train (namely the obstruction due to the bogies) on the flow shear stress at the ballast bed, the results of a computational model are included; they show that a rapid change in the shear stress is related to the position of the protrusions on the underbody. The effect is also shown in on-track experiments, where a pressure jump across the test body is measured. This pressure jump is a measure of the shear stress.[10]

The vibration of the sleeper can also have an influence in the initiation of ballast rotation. It is well known that a body placed on a vibrating surface rebounds over it, reaching a specific height.[11–13] This motion and this height modify the action of a wind gust on the body itself. It has been observed in wind tunnel experiments that the initiation of motion of ballast stones occurs at a lower wind speed with a vibrating floor boundary condition than with a steady one.

Therefore, the dynamic behaviour of the sleeper induced by the passing trains has been measured in terms of the acceleration at the central part, which is the most relevant from the point of view of the ballast. Data on the sleeper acceleration is needed to study this phenomenon in a laboratory (i.e. with a shaker inside a wind tunnel test section). In the past, several on-track experimental studies have been performed to measure the acceleration at the sleeper's shoulder,[14] or at the ballast bed between the sleepers,[15] with the objective of studying the dynamic behaviour of the track; however, in this paper the vibration measurements have the goal of characterizing the sleeper's acceleration at the central zone, which is the most exposed zone for the ballast stones in terms of a wind gust generated by the train, because is the place where the wind speed has its greatest value.

This rest of this paper is organized as follows. A mathematical model is presented in the next section. Then the experimental set-up is described. The analysis of the experimental results concerning pressure measurements, based on the algorithm developed in the section 'Mathematical model' is presented in the section 'Results', together with computational model results, and sleeper vibration characteristics. Finally, conclusions are drawn.

Mathematical model

The effect on the ballast of a wind generated by the passage of a train can be modelled as the effect of wind gusts on stones.[3] When the gust intensity reaches a threshold value (in combination with other effects such as ground vibrations) the smallest, lightest and worst-placed stones start to move and initiate a rotation motion around their trailing supporting point P (Figure 1(a)). to (c) This gust intensity value is the one for which the aerodynamic moment with regard to point P surpasses the gravitational moment (the weight acts as a stabilizing force, acting against the aerodynamic force, in this phase of the motion), as shown in Figure 1(b).

If the gust intensity and duration (that is, the angular impulse exerted on the stone) are large enough, the stone will keep rotating. Should its centre of mass reach the highest possible position (Figure 1(c)), then from this instant onwards the centre of gravity will start to descend, forcing the acceleration of the rotation motion (destabilizing effect). If the initiation of the motion is successful, the stone can hit other stones promoting the initiation of movement, and if this process is repeated, may eventually lead to a saltation process.[7]

The criterion to determine the suitability of a train to operate at a given speed is to establish an upper limit for the angular impulse exerted on the ballast. In order to standardize this criterion, the limit should be independent of the shape and motion of the stone. To fulfill these two conditions, the angular impulse exerted on a standard reference body placed on the ballast is considered. It is placed in a position clearly defined with regard to the sleepers and the tracks, and does not move noticeably during the action of the gust (and thus it is considered as fixed to the ground) (Figure 1(a)). This is the case when a very short and strong gust is considered. The considered dynamic behaviour is very similar to that of a body after a percussive impact.

The determination of the angular impulse exerted on the body during the trains passage is obtained by integration of the net moment of the applied forces (the amount of aerodynamic moment that exceeds the gravitational moment) over the period of time where the net moment is positive; this is a simplification of the real dynamics, but it helps to decouple the results from the actual random values of the size, shape and mass of the stones.

Based on these assumptions, a simple model has been developed to estimate the angular impulse exerted on a standard body by a gust generated by a train. To simplify the explanation this paper considers the motion of a cube, of side l, initially lying on the ground, which can rotate around its trailing edge (Figure 1), under the aerodynamic forces produced by the incoming flow $U_r(t)$, generated by the passage of a train. Assuming that the pressure is reasonably evenly distributed along the windward side p_A and leeward side p_B, that the pressure on the top is the same as in the leeward side p_B, and in the lower side is also p_A (the stagnation pressure), the aerodynamic moment with regard to P, M_{aP} is given by

$$M_{aP} = (p_A - p_B) l^3 k_a \tag{1}$$

where k_a is a factor that takes into account the degree to which the assumptions are valid, e.g. pressure uniformity.

The details of the model development are given in Appendix 2, and the Reynolds number influence in Appendix 3. The angular impulse is given by

$$s_n = \int_{t_1}^{t_2} \left[k_a (p_A - p_B) l^3 - m_p g \frac{l}{2} \right] \mathrm{d}t \tag{2}$$

where t_1 and t_2 are the initial and final instants of the duration of the effective action of the gust. The dimensionless angular impulse is given by

$$S_n = \frac{s_n}{(\rho_a U_T^2 l^3 k_a t_{cn}/2)} = \int_{t_1}^{t_2} \left[c_{pAB}(t) - c_{mge} \right] \frac{\mathrm{d}t}{t_{cn}} \tag{3}$$

where $c_{pAB}(t)$ is the pressure coefficient at A referred to the pressure p_B, and made dimensionless with the dynamic pressure related to the train velocity U_T

$$c_{pAB}(t) = \frac{p_A - p_B}{\rho_a U_T^2/2} \tag{4}$$

t_{cn} is the characteristic time of the gust duration, which is arbitrarily taken as $t_{cn} = 10^{-2}$ s (which is a typical value) and c_{mge} is the coefficient of weight moment with regard to point P, at $t = t_1$ (when the net moment is zero)

$$c_{mge} = \frac{m_p g^* 1/2}{\rho_a U_T^2 l^2 k_a/2} \tag{5}$$

The weight moment coefficient, c_{mge}, increases as the ballast mass, m_p, increases or the train speed decreases. k_a can be determined from the results of tests (e.g. in a wind tunnel) aimed at determining the relationship between the net force and the pressure jump $p_A - p_B$. It is assumed here that $k_a = 0.5$, although the specific value of k_a does not affect the results of the comparison, as will be shown later.

As shown in equation (3), the value of the dimensionless angular impulse, S_n, depends on the value of the weight moment coefficient, c_{mge}. Therefore, the notation $S_n(c_{mge})$ will be used to highlight this point.

$c_{pAB}(t)$ is a measurement of the BTE capability of a train. The erodibility is represented by c_{mge}. A combination of both phenomena should be considered to

analyse the initiation of stone rolling. This is represented by the parameter $S_n(c_{mge})$.

From the measurements of the pressures on the standard reference body (see the next section) taken during the train passes at rail track tests, the variation of the pressure coefficient c_{pAB} (t) can be obtained using equation (4). A schematic representation of the pressure coefficient results is shown in Figure 2.

From the pressure coefficient variation, c_{pAB} (t), the number and intensity of angular impulses generated by the peaks higher than the value c_{mge}, $S_{nj}(c_{mge})$ can be determined, where the subscript j indicates the position in time of each of these angular impulses, as shown in Figure 2. The histogram of the set of values $S_{nj}(c_{mge})$ for several values of c_{mge}, $f(S_n(c_{mge}))$, is shown in Figure 3. Nine bins in logarithmic scale were employed to group the data.

Using the histograms calculated with the data of several passes of the train, an averaged histogram can be obtained, $f_p(S_n(c_{mge}))$, as shown in Figure 4, and the standard deviation at each point can also be computed, which gives a measure of the uncertainty in the evaluation of the averaged histogram f_p.

It will be shown in the section 'Results' that the averaged histogram is a characteristic feature of each train, although the general features (e.g. monotonous decrease with S_n) are quite similar for different trains.

The next step is to analyse the extreme values of the impulse, which can give rise to the motion of stones. The extreme impulse is the one that appears just once (because it is the greatest one), which is denoted here as the singular extreme impulse, S_{nx}. As an example, in Figure 4 the position of the singular extreme impulse values S_{nx1}, S_{nx2}, S_{nx3} are labelled as P_1, P_2 and P_3, respectively, which correspond to stones with weight moment coefficients arbitrarily taken as $c_{mge}=0.2$, 0.4 and 0.6, respectively. It should be noted that the lower the weight of the stone, or the higher the speed of the train (c_{mge} is lower), the greater the singular extreme impulse S_{nx} exerted by the gust. Obviously, there is a maximum limit for c_{mge}, $c_{mge\,max}=\max\,[c_{pAB}\ (t)]$, beyond which there are no more peaks that can contribute to the impulse (Figure 2).

The next step is to find out if these singular extreme impulses (S_{nx1}, S_{nx2}, S_{nx3}) are large enough to give rise to the critical angular velocity, $\dot{\theta}_{crit}$, needed to initiate the stone's rolling motion. The impulse required for a given stone to achieve the critical velocity, s_{ncrit}, can

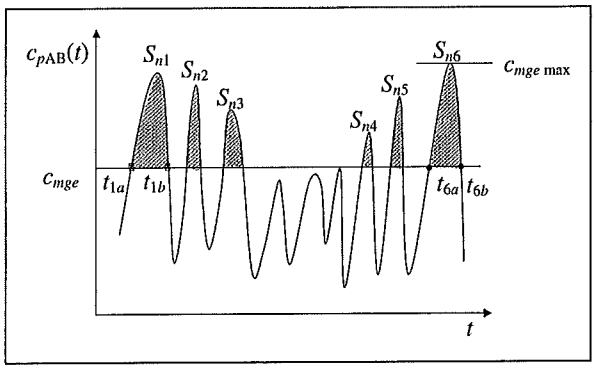

Figure 2. Sketch of the variation with time, t, of pressure coefficient, c_{pAB}, during a typical train pass. The shaded areas are the impulses S_{nj} corresponding to the pressure peaks j ($j=1,\ldots,6$) which exceed the level c_{mge}. t_{ja}, t_{jb} are the limits of the time intervals where the applied net moment is positive in each pressure peak.

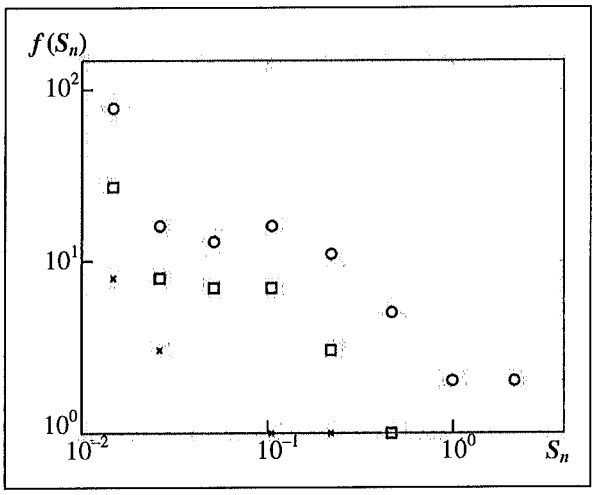

Figure 3. Typical histogram of dimensionless angular impulse $f(S_n)$, obtained in experiments for one pass of the train, for $S_n(c_{mge})$, when the pressure peaks exceed the levels c_{mge}, as given by the following key: $c_{mge}=0.2$ (circles), 0.4 (squares), 0.6 (crosses).

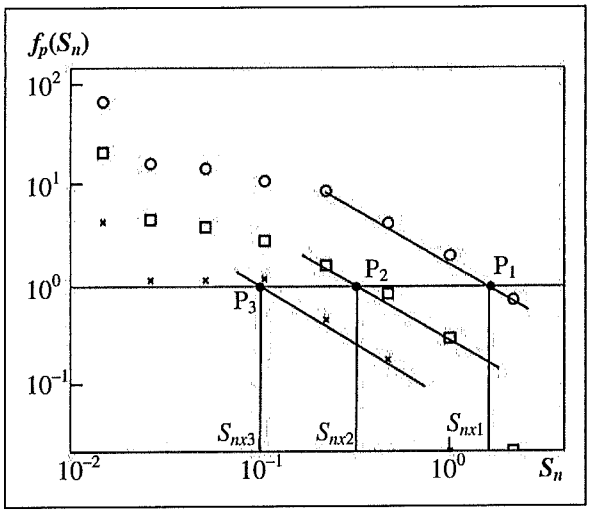

Figure 4. Averaged histogram of the dimensionless angular impulse, f_p (S_n), for several values of the level c_{mge} ($c_{mge}=0.2$, circles; 0.4, squares; 0.6, crosses). Data from 20 passes of the train have been considered. S_{nxi}: singular extreme impulse value corresponding to the cases $c_{mge}=0.2$ ($i=1$); $c_{mge}=0.4$ ($i=2$), $c_{mge}=0.6$ ($i=3$), labeled P1, P2 and P3, respectively.

be obtained (Appendix 2) by using equations (14) and (16) and recalling that in this case $\dot{\theta}(t_2) = \dot{\theta}_{\text{crit}}$, then

$$s_{n\text{crit}} = I\dot{\theta}_{\text{crit}} = I\sqrt{\frac{2m_p g\Delta h}{I}} = \sqrt{2m_p g\Delta h I} = \sqrt{2m_p g\Delta h m_p r_{g\text{P}}^2} = m_p\sqrt{2g\Delta h r_{g\text{P}}^2} \tag{6}$$

which can be rewritten in dimensionless form by using the definition in equation (3)

$$S_{n\text{crit}} = \frac{s_{n\text{crit}}}{\rho_a U_T^2 l^3 k_a t_{cn}/2} = \frac{m_p\sqrt{2g\Delta h r_{g\text{P}}^2}}{\rho_a U_T^2 l^3 k_a t_{cn}/2} = c_{mge}\frac{2\sqrt{2}}{t_{cn}} t_{crg}\left(\frac{\Delta h}{l}\right) = c_{mge}\frac{t_{crg}}{t_{cn}}\left(2-\sqrt{2}\right) \tag{7}$$

where $\Delta h = (\sqrt{2}-1)l/2$ for the cubic shape considered here. Assuming $l \approx 3\,\text{cm}$, $k_I \approx 1$, then $t_{crg} \approx 0.12$, $\Delta h/l = 0.21$ and therefore

$$S_{n\text{crit}} = 7.1 c_{mge} \tag{8}$$

that is, the critical impulse increases proportionally to the weight moment coefficient (the greater the weight of the stone, the larger the angular impulse required). This result is for a cubic stone. However, for the case of a stone of another shape a similar process can be followed to obtain an expression similar to equation (8). The cubic stone is simply an example to explain the method.

For this purpose let us consider the combination of the two results obtained so far, the singular extreme impulse generated by the train gust, and the critical impulse for the initiation of the stone's rolling movement. The experimental values of the singular extreme impulse, as a function of the weight moment coefficient $S_{nx}(c_{mge})$, is a property of the train's aerodynamics (and of the shape of the stone or test object), and the critical impulse in equation (8) is dependent on a stone's characteristics. The variation with the weight moment coefficient is shown for three trains in Figure 5. The singular extreme value generated by train 't', $S_{nx,\text{Train}t}$, decreases as the weight moment coefficient, c_{mge}, increases (due to an increase in mass increase or a decrease in the train's speed), while the impulse needed to start the rolling process, $S_{n\text{crit}}$, increases with c_{mge}.

The limit of stability is attained when both lines, $S_{nx}(c_{mge})$ and $S_{n\text{crit}}(c_{mge})$, cross at $c_{mge} = c_{mgeL}$. For stones with $c_{mge} < c_{mgeL}$, the effective impulse (singular extreme impulse $S_{nx,\text{Train}t}$) is larger than the critical one corresponding to the critical weight, $S_{n\text{crit}}$, and, therefore, the conditions for the rolling process are met.

To obtain a determination of $S_{n\text{crit}}$ (which depends on the mass, shape and size of the stone) a detailed analysis of the stone is required. However, to compare the effect on the ballast of different trains, only the relative position of the train's characteristic curves, $S_{nx,\text{Train}t}(c_{mge})$, is needed. Consider, for instance, that the limit appears at Lb, which is the value of the extreme impulse, S_{nx}, generated by train 'b' at the point of stability limit, in this case $c_{mge} = 0.4$ (Appendix 4). In relation to this train, train 'a' is on the stability side (it causes less erosion than train b), and train 'c' is on the unstable side (it causes more erosion than train b).

Concerning the critical impulse defined in equation (7) or equation (8), it should be noted that the assumption that the stone does not appreciably move during a short-duration gust may not always be completely valid. Indeed, the duration of the gust, t_{cn}, could be of the same order as t_{crg}, the characteristic time of a stone in moving from $\theta(t_1) \approx \theta(t_2)$ and reaching $\theta_{\max}$ at t_3, $\theta(t_3) = \theta_{\max}$. To take this effect into account, in equation (7) a so-called efficiency factor, k_s (to be determined from experimental tests), should be included

$$S_{n\text{crit}} \equiv k_s c_{mge}\frac{t_{crg}}{t_{cn}} \tag{9}$$

However, this factor is not needed to make the comparative study depicted in Figure 5. In fact, the limit value, Lb, between erosional and non-erosional trains can be provisionally established in the light of the amount of knowledge obtained from the performed experimental studies.

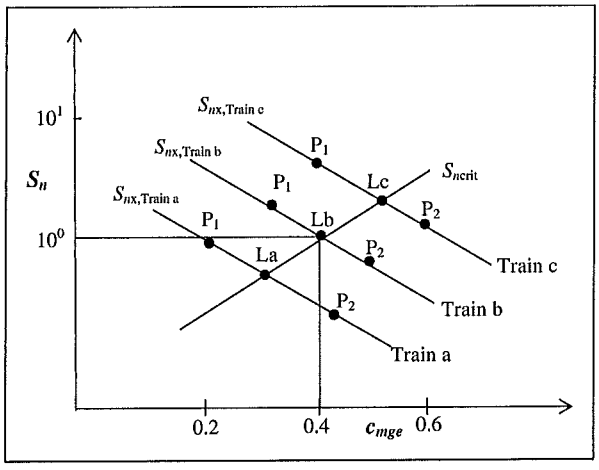

Figure 5. Variation of the dimensionless angular impulse S_n with the weight moment coefficient, c_{mge}. $S_{nx,\text{Train}t}$: singular extreme impulse generated by several trains t = a, b, c. $S_{n\text{crit}}$: critical impulse required to start the rolling motion of a given stone. La, Lb, Lc: stability limit points for the three trains, respectively. P1: singular extreme impulse for a stone with $c_{mge} < c_{mgL}$ (L = La, Lb, Lc respectively for each train), successful rolling. P2: singular extreme impulse for a stone with $c_{mge} > c_{mgL}$, unsuccessful rolling.

Experimental set-up

The experimental approach selected to study the effect on the ballast of the flow generated by the train is the measurement of the pressure load due to this flow acting on a standard reference body (a cylinder with two parts, of different cross-section) placed on the ballast. The body consists of two different parts, one is a semi-cylinder and the other a vertical wall, both of them equipped with pressure taps. Furthermore, the acceleration of the vibrational motion in the centre of a sleeper is also measured, and the instants when the train wheels pass over the stone model are also recorded, for data synchronization. The idea behind having two different parts is to create the possibility to study the influence of the shape.

The experiments were carried out during the period between 26 October 2010 and 23 March 2011, in two sessions, one on each track of the double-track railway at kp 69 + 500 on the Madrid – Barcelona High Speed Line. On track 1, the level of the ballast bed was lowered with regard to the level of the rail base, in order to let the surrounding air flow into the space between both rails, or flow out from this space. On track 2, the space between the ballast bed and the rail base was occupied by the ballast stones. At the beginning of each session the experimental equipment was installed on the track at night, outside of commercial operation time.

The distribution of the equipment is shown in Figure 6. The standard reference model was placed buried in the ballast bed, between two sleepers (Figure 7(a)) and (b) at a point coinciding with a catenary pole. Two accelerometers were screwed to a metallic base plate (Figure 7(b)), which was fixed using two screws to the sleeper behind the model, relative to the train direction. A light barrier, consisting of an emitter and a reflector, was also installed. The reflector was attached to the model box at the side facing the external rail. The emitter was attached to the catenary pole. In this configuration, the wheels of the bogies passing over the stone model are detected when they cut the light barrier.

Description of the equipment

Pressure measurements were performed using the discussed standard reference body (an idealization of a stone lying on the trackbed or on a sleeper), which is composed of two cylindrical parts, each one 19 cm long, shaped with a different cross-section (Figure 8). Figure 8(a) to (c) One part has a 6 cm diameter semi-cylindrical cross-section (Figure 8(a)), and the other part has a 3 cm high and 2 cm wide rectangular cross-section (like a thick vertical wall, Figure 8(c)). In order to establish an as close as possible two-dimensional aerodynamic configuration, two vertical walls were placed parallel to the main flow direction at both sides of the body, and also

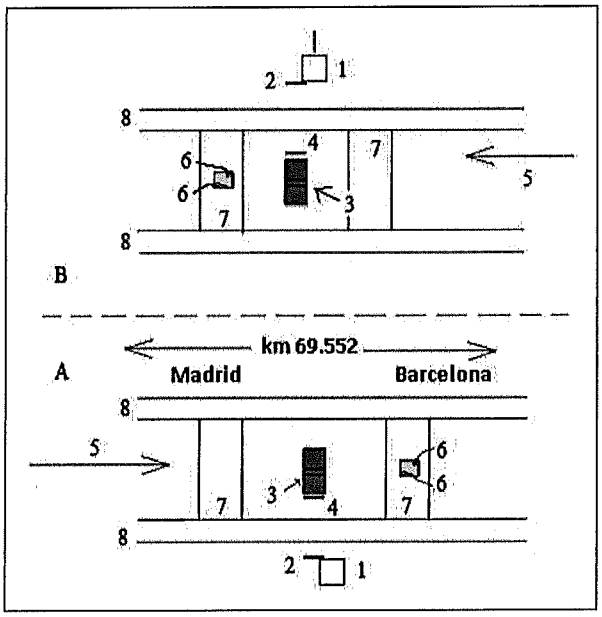

Figure 6. Sketch of the locations of equipment. 1, catenary pole; 2, emitter; 3, standard reference body; 4, reflector; 5, train motion direction; 6, accelerometer; 7, sleeper; 8, rail. A, track 1; B, track 2.

another one at the central section between both parts. The reference body was mounted on top of a 40 × 17 × 10 cm parallelepiped box, on a plane wooden surface, which was level with the upper surface of the sleeper and was considered as a reference plane for the flow. Inside this box, the instrumentation (pressure transducers and the accelerometer amplifiers) were accommodated, isolated from the walls by using foam, in order to avoid the effect of vibrations of the trackbed on the pressure transducers. The wooden walls also helped to isolate them from vibrations. The box was buried in the ballast bed, in the space between two sleepers, which were 0.5 m apart.

The positions of the pressure taps on the standard reference body are a compromise between the simplicity of the test and the need for appropriate data to feed theoretical models. When possible, the pressure taps were placed in pairs in order to provide some redundancy, thus avoiding single point failures, which could impede the success of the measurement campaign that had to be carried out in a harsh working environment. In fact, it allowed data to be obtained during periods of time in which a temporary failure of one of the redundant pressure channels occurred. The similarity between the measurements of redundant pressure channels supports the assumption of the two-dimensional flow, at least in the centre of each cylindrical part, despite the turbulent character of the flow.

Following this philosophy, at the semi-cylindrical part of the body five pressure taps were arranged, as shown in Figure 8(a). The reference pressure tap (TR) was placed at the lowest part of the semi-cylinder and faced the incoming flow produced by the passing

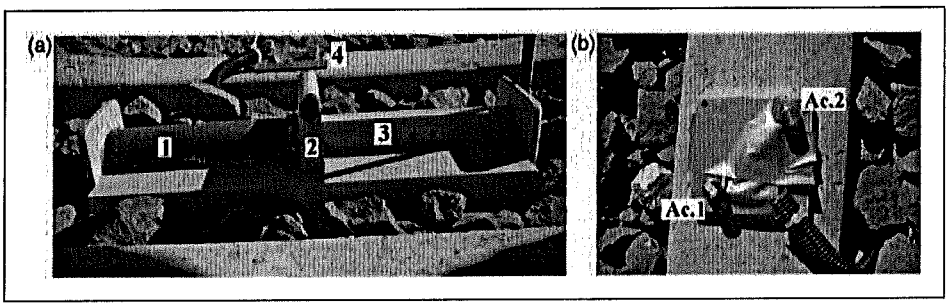

Figure 7. (a) Photograph of the standard reference body and the instrument box in place. 1, semicylindrical section; 2, Pitot tube; 3, vertical wall section; 4, accelerometers mounted on a plate and (b) photograph of the accelerometers 1 and 2 placed on the sleeper.

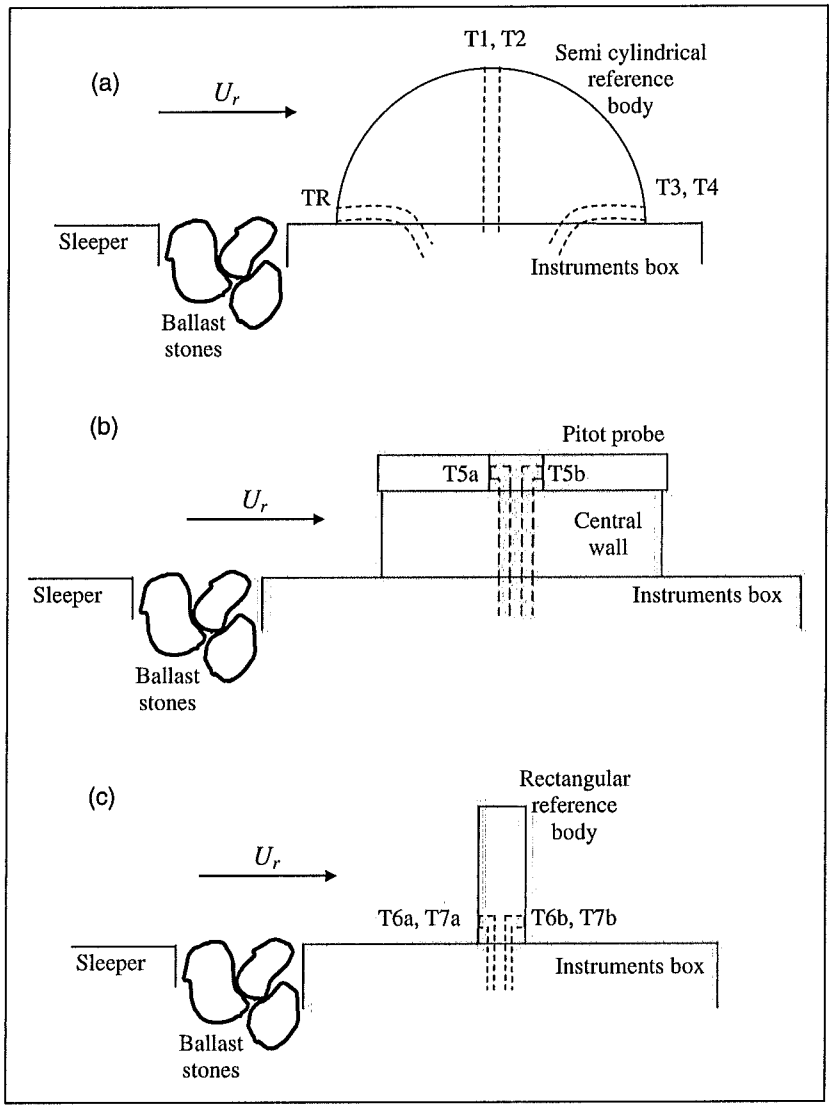

Figure 8. Sketches of the parts of the standard reference body with pressure tap positions: (a) semi- cylindrical section; (b) Pitot tube; and (c) vertical wall.

train, U_r. The twin taps T1 and T2 were placed together, 2 cm apart, on the upper part of the semi-cylinder, while the twin taps T3 and T4 were placed at the opposite side, and at the same level as the reference tap. The pressure differences between the reference point TR and points 1, 2, 3 and 4 were measured by connecting the pressure taps T1, T2, T3 and T4 to the high-pressure ports of four differential pressure transducers and the four low- pressure ports were connected to the reference tap.

Midway between the two parts of the test model a kind of Pitot flow-direction probe with two opposite taps (T5a in the windward side of the model and T5b in the leeward side) was placed 50 mm higher than the

reference flat plane (Figure 8(b)). At the base of the vertical wall, the pressure taps T6a and T7a were placed at the windward side of the wall and T6b and T7b at the leeward side of the wall. T6 and T7 are also twin taps to provide redundancy (Figure 8(c)).

The differential pressure sensors were Sensor Technics Id.BTEM5P350D4C type, with a ± 35 kPa measurement range, and a 4–20 mA current loop output. The measurement range of the pressure sensors was several times the expected measurement range, to allow for a margin to avoid damaging the sensors, and robustness to survive the several months placed in the track.

In summary, the standard reference body was instrumented with seven differential pressure transducers to measure the following pressure signals: $p_1 - p_r$, $p_2 - p_r$, $p_3 - p_r$, $p_4 - p_r$, $p_5 - p_r$, $p_6 - p_r$ and $p_7 - p_r$. As previously mentioned, the first four transducers were for the semi-cylinder pressure taps, the fifth one for the Pitot probe taps and the remaining two for the vertical wall taps. In this case, as outlined in the section 'Mathematical model', the pressure coefficient, c_{p0j}, is defined as

$$c_{p0j} = -\frac{p_j - p_r}{\rho_a U_T^2/2}$$

where $j = 1, 2, 3, 4, 5, 6, 7$. This pressure coefficient is not the one usually used in the field of aerodynamics, where the reference pressure p_r is the static pressure of the incoming flow, and the dynamic pressure is defined in terms of the incoming flow speed, since both are difficult to determine in the space between the railroad track and the lower parts of the train. Note also that the usual aerodynamic pressure coefficient has the opposite sign to that of the coefficient used in this paper. For pressure coefficients $j = 1$, 2, 3 and 4 the reference pressure is p_R. For pressure coefficients $j = 5$, 6 and 7, the measured point is labelled with the subscript 'a', and the reference pressure with the subscript 'b'. Typical peak pressures measured were 3 to 4 kPa and the manufacturer's quoted uncertainty is 0.2% of the full- scale output, therefore the measurement error was approximately 2%.

Aiming to obtain experimental data that can help the study of the action of the sleeper's vibration on the initiation of the rotation of the ballast lying on it, the vertical acceleration at the centre of the sleeper was measured by using two redundant accelerometers screwed to a steel plate, which was fixed to the sleeper placed immediately downstream of the stone model (see Figure 7). The measuring range of the accelerometer (KS-77C-100/01) is from -60 g to $+60$ g with a sensibility of 0.1 V/g. Based on aerodynamic considerations, it was estimated that the most exposed situation for the ballast to initiate the motion was when it was placed on the midpoint of the sleeper. The amplitude of the sleeper motion was also estimated to have its greatest value at this point. Therefore, this position was considered to be the one with the worst conditions, and, thus, it was selected as the most appropriate location for the accelerometers.

The time tagging of the pressure and acceleration signals measured during each pass had to be made independent of the train speed, U_T, to allow for comparison and averaging to be performed. To achieve this, the measurements were synchronized by transforming the time tagging to the corresponding longitudinal position along the train, $x = tU_T$. Using this new variable, the pressure and acceleration peaks could be correlated with the geometry of the train's underbody. To carry out this comparison, the instants of wheel passes were detected by using the previously discussed SENSICK WL 12-2 light barrier.

All the signals generated by the measurement equipment on the track were transmitted via a 50 m cable to a NI USB-6210 data acquisition system (DAQ). The DAQ was connected through a USB port to a laptop, running a LABVIEW programme that controlled the data acquisition process. By using a modem, the data were downloaded from the IDR/UPM Control Centre (CC) in Madrid to post-process them. A Grelco VD-305, 30 V, 5 A, power supply was used to supply power to all the instruments. The whole system was protected against power failures by a SAI Belkin F6C425, 425 VA, 255 W. All this acquisition and communication equipment (uninterruptable power supply) was placed inside the control centre. The data acquisition was performed at a 16 kHz sample rate. A 10 s measurement period was recorded starting 2 s before the instant when the train's first wheel interrupted the light barrier. The power spectrum of the pressure signal shows a very low value of the spectral density for frequencies larger than 1 kHz. As the sampling was carried out at 16 kHz, no additional precautions were taken.

Thanks to the control programme and remote operation architecture, the system worked continuously (24 h a day, 7 days a week). Data of the passes of several train types were recorded. Four train models (TMs) were selected for analysis. Due to railway administration confidentiality regulations, their identity will not be disclosed and they are just labelled as TM = 1 to 4. Fortunately, this has no influence on the main result of the work, which is to compare several train types. The only information about a train's underbody that has been disclosed for use in this paper is that the bogies pass instants of a given train model separately, to analyse the variation with the longitudinal position of the pressure coefficient.

Data processing

Differential pressure, acceleration of the sleeper, light barrier output and time tag data, for each train pass, were saved onto a file, then compressed, downloaded

via the Internet from the IDR/UPM Control Centre, and decompressed.

Post-processing of a pass data consisted of the following steps.

1. A zero-bias correction was performed: the pressure and acceleration average during periods with no train passes was subtracted from the original pressure and acceleration signals, respectively.
2. The train was identified by counting the number of assumed axles.
3. The train speed was calculated from the distance between assumed axles and the train length.
4. The reference system for the measurements was transformed from time t to longitudinal position x.
5. The pressure coefficients and the sleeper acceleration were obtained.
6. The data signals were low-pass filtered (300 Hz cut-off frequency for pressure coefficient and acceleration signals, the procedure to determine this value will be explained in the next section) numerically to remove high-frequency fluctuations and noise.

More than 5000 passes in a total of 145 measured days and 40 Giga bytes of data were recorded.

Results

The quality of the pressure measurements and the effect of the noise can be appreciated in Figure 9(a), and (b) where a short interval of time, converted to coordinate x, of channels 1 and 2, that is $c_{p01}(x)$ and $c_{p02}(x)$, is plotted as an example. Similar results are obtained in the case of the other twin channels. The good agreement between the measurements of the channels can be observed, which also gives great confidence in the quality of the measurements.

The effect of the number of train passes, N_p, used to calculate the ensemble average at each point along a train, or signature of the train, is shown in Figure 9(b). All the tested trains show a similar signature, although with different characteristics. Note the small difference in the results for $N_p = 10$ and $N_p = 20$. Some of the sudden jumps are associated with the elements of the geometry of the train's underbody, e.g. bogies. This information can help to refine the aerodynamic design of the underbody.

The results obtained for several pressure channels are displayed in Figure 10(a) and (b), separated into two plots to distinguish between them more clearly. The similarity of the shape (signature) among all the channels can be appreciated, they only differ in magnitude. This similarity of the ensemble averages of different channels suggests the existence of a deterministic component in the pressure signal, which can be associated with the geometry of the train's

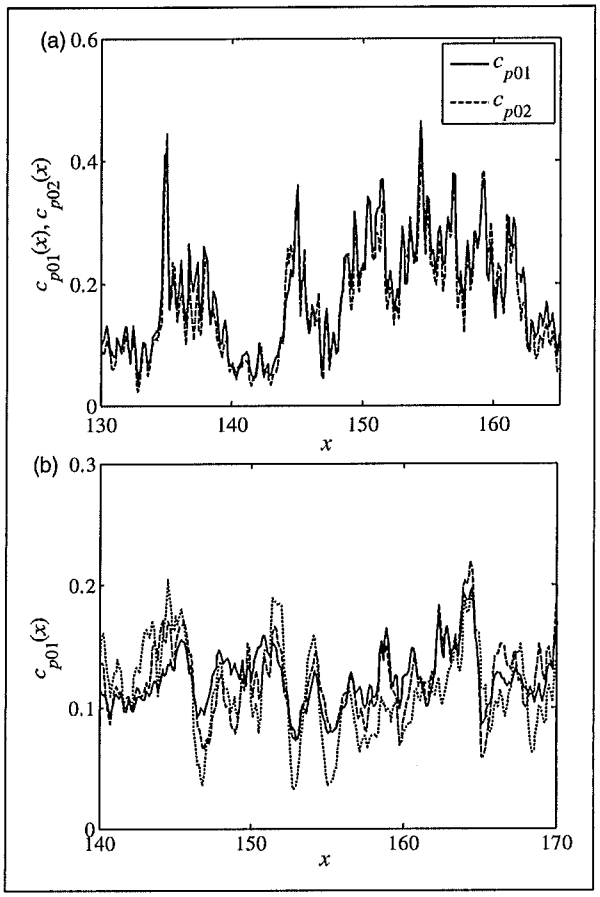

Figure 9. (a) Variation with the longitudinal position x (in metres) of the pressure coefficient of the twin channels $c_{p01}(x)$ and $c_{p02}(x)$, for a train passing over track 1. Only a part of the train is shown to allow for a better comparison and (b) variation with the longitudinal position, x (in metres), of the pressure coefficient, $c_{p01}(x)$, obtained by ensemble average of a number, N_p, of passes of the same train. $N_p = 5$ (dotted line); $N_p = 10$ (dashed line); $N_p = 20$ (solid line).

underbody. Regarding this geometry, the time taken for the passage of the bogies over the standard reference body, measured with the light barrier, are presented in Figure 10. The case of the pressure variation as a function of time of the train shown in Figure 10, which is the train type that the authors are able to disclose in this paper, there is no clear correspondence between the bogie passes and the pressure peaks, which could be due to the lack of large protrusions from the underbody. A simplified numerical computational model of the flow in the underbody region of another train will be presented later in this section which shows more clearly this correspondence. In Figure 10, at the start and the end of the train, the potential flow associated with the train nose, and the largest gust due to the wake, respectively, can also be observed. The effect of underbody protrusions will be shown later, with the help of a computational model.

From plots of single passes as in Figure 9(a), or as sketched in Figure 2, dimensionless impulse histograms are obtained for the different trains. From these

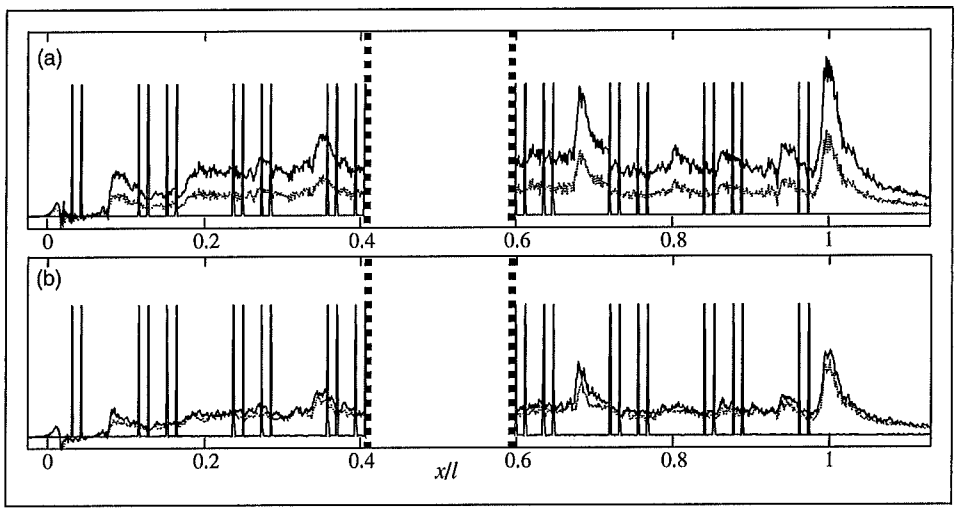

Figure 10. Variation with the longitudinal position, x, of the pressure coefficients $c_{p0j}(x)$ obtained as the ensemble average of 20 passes, (a) $c_{p01}(x)$ (solid line), and $c_{p03}(x)$ (dotted line); (b) $c_{p05}(x)$ (solid line), and $c_{p06}(x)$ (dotted line), for a model of train. $c_{p02}(x)$, $c_{p04}(x)$, $c_{p07}(x)$ are not shown as their results practically coincide with their twins. Pulses are a representation of the longitudinal position of the bogies. l: length of the train.

data, averaged histograms are obtained and plotted for two trains and two tracks in Figure 11(a) to (d). The values of the singular extreme impulse S_{nx1}, S_{nx2}, S_{nx3} are lower for train 1 than for train 2 whatever the track, and lower for track 1 than for track 2 whatever the train. The characteristics of the train's underbody are different for each train type, and thus the effect of the flow on the track will also be different. As previously mentioned, on track 1, the level of the ballast bed was lowered with respect to the level of the rail base, so the surrounding air can flow from the space between both rails, and the mean pressure level on the track can be decreased. On track 2, this space between the ballast bed and the rail base was occupied by the ballast stones. Therefore, the air could not flow out the space between both rails; the air flow from the surroundings towards the space between both rails was restrained, and therefore the inner flow was more intense, leading to pressure peaks higher than on track 1. From now on the notation $S_{nx1} = S_{nx}(c_{mge} = 0.2)$, $S_{nx2} = S_{nx}(c_{mge} = 0.4)$, $S_{nx3} = S_{nx}(c_{mge} = 0.6)$ is employed, for brevity.

As the total number of averaged histograms obtained –the number of pressure channels (seven) times the number of trains (four) times the number of tracks (two) for each c_{mge}– is too large to include in this paper, the results are summarized by focusing only on the single extreme impulse for each train, $S_{nx,\mathrm{Train}\,i}(c_{mge})$, for just two values of the weight moment coefficient, $c_{mge} = 0.2$ and 0.4, but paying attention to all pressure taps, T1 to T7, and the passes for the two tracks, V1 and V2, as shown in Figure 12(a) to (d). The measurements from pressure taps T1 and T2 are considered in Figure 12(a). The results from both twin taps almost coincide in most cases. The single extreme impulse values for track 2 are higher than those obtained for track 1, which can be traced back to the difference in the level of ballast with respect to the rail base, as previously mentioned. Similar behaviour occurs when comparing the influence of the weight moment coefficient, c_{mge}. For small values, $c_{mge} = 0.2$, the extreme impulse values are larger than in the case $c_{mge} = 0.4$, as expected.

The same comments can be applied to Figures 12(b), 12(c) and 12(d), where the results for the other pressure taps are presented, showing that the extreme values for the pressure jumps associated with drag forces, c_{p03}, c_{p05}, c_{p06}, (and their twins) are about four times lower than the pressure jump corresponding to lift forces, c_{p01}, or c_{p02}. Therefore, in this reference body the effect of lift is significantly greater than the effect of drag. Anyway, the relative erosional effect is the same whichever pressure tap is considered, that is, the singular extreme impulse increases as the train model increases, whichever pressure tap, track, or weight moment coefficient is considered.

To give an example of a possible comparison among the several train types considered, a horizontal line has been included in Figure 12, which indicates the limit value of the singular extreme, S_{nx2} (following the explanation given in Appendix 4, the value $c_{mge} = 0.4$ was chosen as a baseline for reference), for the pressure taps T1 and T2, $S_{nx2} = 1$, and for T3 and T6 (or their twins), $S_{nx2} = 0.25$. According to this figure, train models TM 1 and TM 2 are compliant with this limit, TM 3 is in a marginal position and TM 4 is beyond the limit, $U_T = 80$ m/s, on track V1.

In order to clarify the effect of underbody protrusions on the shear stress of the flow at the ballast bed, some experimental results were compared with computational results obtained from a two-dimensional model. The geometry of the computational model (in a reference frame attached to the train) consists of a channel with the upper wall fixed and the lower

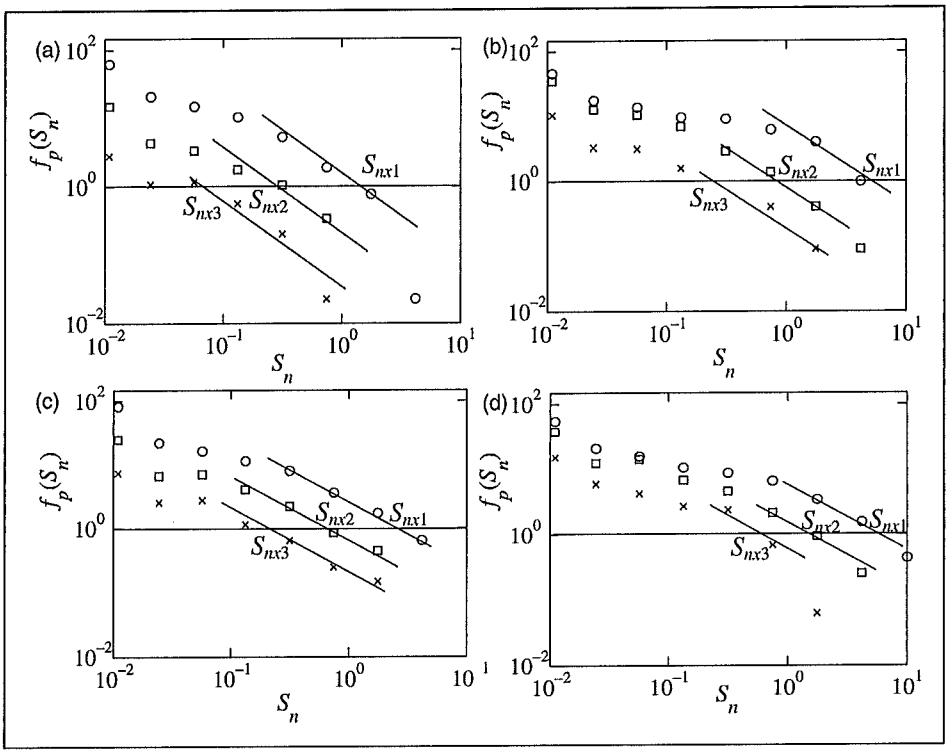

Figure 11. Averaged impulse histograms, $f_p(S_n)$, for two values of the weight moment coefficient, c_{mge}, for two different trains passing over track 1 and track 2: (a) 44 passes of train 1 over track 1; (b) 22 passes of train 1 over track 2; (c) 20 passes of train 2 over track 1; and (d) 16 passes of train 2 over track 2. Solid straight lines help to show the almost linear variation of the results in the range considered. $c_{mge} = 0.2$ (circles), 0.4 (squares), 0.6 (crosses).

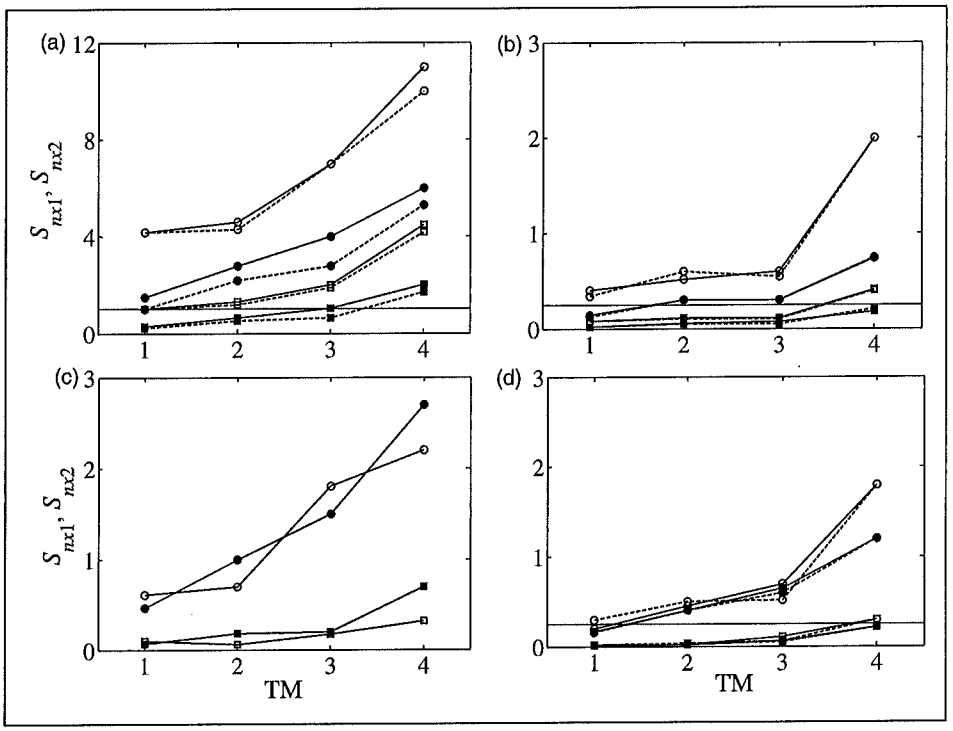

Figure 12. Singular extreme values S_{nx1}, and S_{nx2}, for four train models (TM = 1 to 4), tracks V1 and V2 (V1 full symbols, V2 open symbols), weight moment coefficients ($c_{mge} = 0.2$, circles; 0.4 squares): (a) solid line, pressure tap T1; dashed line, T2, (b) solid line, pressure tap T3; dashed line, T4, (c) solid line, pressure tap T5 and (d) solid line, pressure tap T6; dashed line, T7. S_{nx1}, S_{nx2}: singular extreme impulse values for $c_{mge} = 0.2$ and 0.4, respectively.

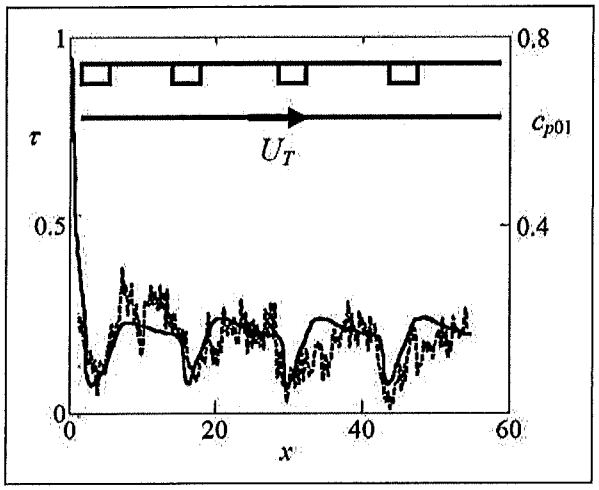

Figure 13. Variation with the longitudinal position, x, of the shear stress (solid line), τ (units: kg/(m·s^2)), on the lower plane wall of a two-dimensional channel; and of the pressure coefficient (dashed line), $c_{p01}(x)$, obtained as an ensemble average of 20 passes of the same train. x is made dimensionless with the channel width. The lower wall is moving from left to right with speed U_T with respect to the fixed upper wall, which contains rectangular protrusions (as a representation of the bogies) separated from each other by a constant distance, as shown in the sketch.

wall moving parallel to itself from left to right at a speed U_T with regard to the upper wall (see insert in the upper part of Figure 13). The lower wall is flat (simulating the track bed), whereas the upper wall has rectangular protrusions attached (simulating the bogies of the train) and separated from each other at a constant distance. The configuration is a variation of turbulent Couette flow between two plane parallel walls;[16] however, the upper wall has periodic protrusions, which represents in a simplified manner, the configuration between the train's underbody and the track, in a train reference frame. The shear stress on the track bed is a measure of the action of the fluid on the ballast. The shear stress on the lower wall suddenly changes at the positions of the protrusions (bogies or specific elements under the train), as is shown in Figure 13. It can be appreciated that the periodic variation with time of the measured pressure coefficient is synchronized with the passes of the protrusions, appearing as a peak in the middle of the distance between two consecutive protrusions, and decreasing again with the next protrusion. This is due to the flow acceleration (in the train reference frame) at the region close to the bogie, which reduces the flow speed relative to the track, thus decreasing the shear stress at the lower wall (the trackbed). The numerical results show a qualitative good agreement with the results of the on-track experiments, if the signal pattern of the pressure coefficients of the taps of the reference body is considered (see experimental measurements of $c_{p01}(x)$ in Figure 13). The pressure coefficient across a small wall perpendicular to the floor is proportional to the shear stress.[10] The

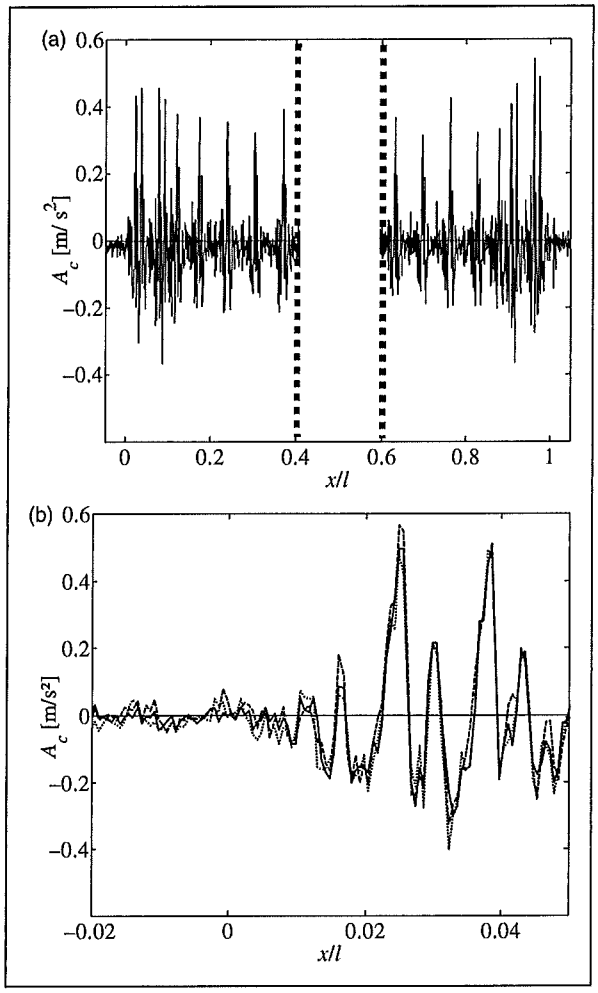

Figure 14. Variation of the acceleration, A_c, at the centre of the sleeper, with the longitudinal position, x, divided by the train length, $l = 400$ m, (a) for the whole train and (b) for the initial part at the nose, for three passes of the same train at 83 m/s. $x = 0$ is the position of the nose of the train. A low-pass filter is applied (300 Hz).

decrease in the shear stress at the trackbed during the passes of the protrusions, which was observed both in the experiments and in the numerical simulation, is in contradiction with some researchers' intuition, who associate the flow acceleration below the train with an increase in the shear stress. If the train's underbody were completely flat, the shear stress would be almost constant and have a reduced mean level. The peak at $x = 0$ in Figure 13 (computational results) should be disregarded, as it corresponds to the starting conditions of the flow.

To collect data to study the possible effect of the sleeper vibration on initiation of ballast rolling, the acceleration at the centre of the sleeper, excited by passing trains, was also measured. The variation with time of the acceleration at the centre of the sleeper, filtered by a low-pass moving average filter (with a cut-off frequency of 300 Hz), is presented in Figure 14(a) and (b). The large periodic pulses are related to the effect of the bogies passing above the shoulder of the sleeper where the accelerometers are

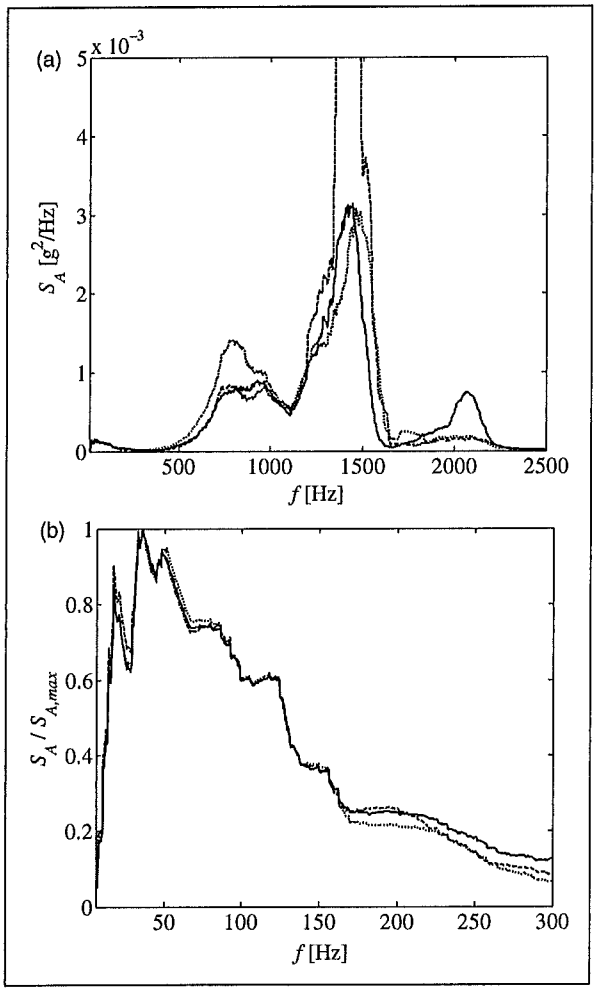

Figure 15. Spectral density of the acceleration, S_A, at the centre of the sleeper measured with accelerometer 2, for three passes at 83 m/s of the same train model (a) spectral density variation with frequency, f, up to 2500 Hz and (b) variation with the frequency up to 300 Hz of the spectral density divided by the maximum value of the spectral density, $S_{A,max}$, in the low-frequency range ($f < 300$ Hz).

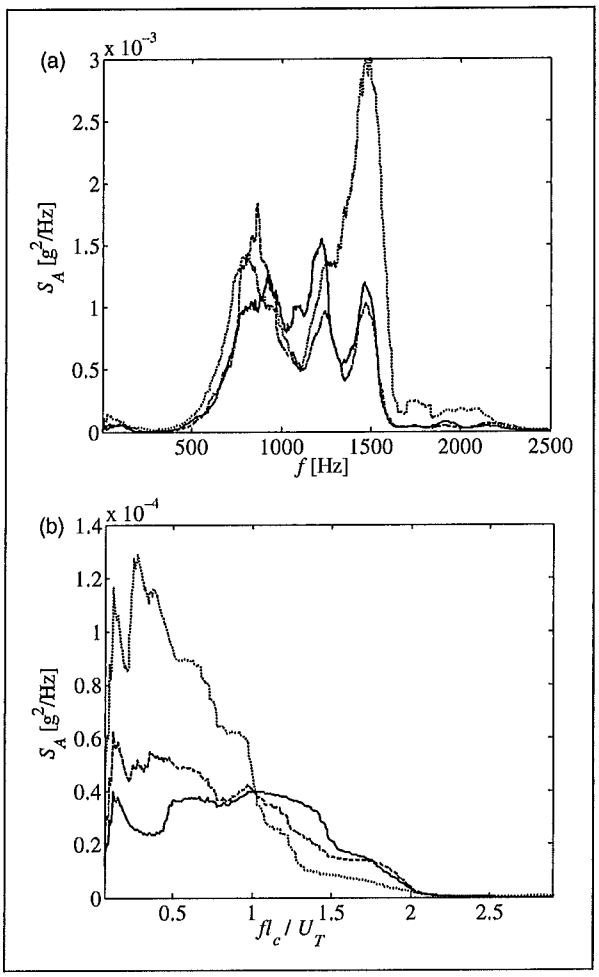

Figure 16. Spectral density of the acceleration, S_A, at the centre of the sleeper measured with accelerometer 2, for three passes at 59 m/s (dotted line), 69 m/s (dashed line), and 83 m/s (solid line) of the same train model (a) spectral density variation with frequency, f, up to 2500 Hz and (b) spectral density variation with dimensionless frequency up to 3. $l_c = 0.65$ m; U_T: train speed. A low-pass filter is applied (300 Hz).

placed. It is understood that the motion of the stone over the sleeper will be driven by the low-frequency part of the acceleration spectrum. Also, the existence of a train signature in the sleeper's vibration spectrum could help to analyse this problem. This consideration leads to the problem of determining the cut-off frequency, which was obtained in the following way. The variation with the frequency of the spectral density of the sleeper acceleration for three distinct passes of the same train model at the same speed is plotted in; Figure 15(a) and (b) two regions with different types of behaviour can be clearly observed. Below a frequency of approximately 300 Hz the curves are almost coincident, which suggests the existence of a deterministic range. In Figure 15(b), this deterministic zone for frequencies below approximately 200 Hz can be observed more clearly. Above this frequency, the spectral densities for different train passes at the same speed (Figure 15(a)) are not coincident, but rather show random contributions, which can be associated with a non-deterministic behaviour. To establish this observation further, a time domain analysis can be used as follows.

The variation with time of the acceleration filtered by a 300 Hz low-pass filter is compared for three train passes at the same speed in Figure 14(b). A good agreement between all measurements is observed, which suggests, as previously mentioned, that the response of the track is deterministic at least in this low-frequency range.

The quality of the measurements was also checked by comparing the outputs from both accelerometers. The comparison showed a good agreement between the readings of both channels.

The influence of the train's speed on the spectral density can be analysed based on the types of peaks of the spectral density functions. The variation of the frequency of the spectral density of the sleeper acceleration for three passes of the same train model as a function of train speed is presented in Figure 16(a)

and (b). Some of the peaks appear at the same frequency independent of the speed of the train, which suggests that this part of the spectrum is related to intrinsic characteristics of the sleeper and track system (i.e. the peaks at 1250 and 1500 Hz). In the range between 700 and 1200 Hz, there is no clear dependency of the frequency of the peaks of the spectral density on train speed, so this part of the spectrum is random distributed. In the deterministic range ($f < 300$ Hz) some dependence of spectral density with train speed can be observed. If a dimensionless frequency is used (see Figure 16(b)), by using the train speed, U_T, and a characteristic distance $l_c = 0.65$ m, two different deterministic regions can be observed separated by $f \times l_c / U_T = 1$. The influence of the train speed on the spectral density is different at either side of this limiting frequency. On one side the spectral density increases with train speed whereas on the other side it decreases. As previously mentioned, this deterministic part of the spectrum is simply the zone of relevance to study the initial rotation of ballast stones, as the vibration of the sleeper can influence the creation of rotational movement. If an analysis of the initial rotation of the ballast stones lying on the sleepers were required, the contribution of the different parts of the acceleration spectrum could be included in the dynamic model, but at this track/train interoperability standardization phase, the hypothesis considered is that the stones are not supposed to be on the sleepers, which are assumed to be in a clear state.

The next step in the study of the acceleration contribution analysis would be to carry out specific experiments focused on determining the coefficient of restitution[12] of the stones in the sleeper/ballast system at the vibrating frequencies that excite the resonant jumping of the stones. With the sleeper acceleration information obtained in these experiments, the maximum height reached, h_m, by the ballast stone for the exciting frequencies could be calculated. On the other hand, from on-track experiments,[3,17] wind tunnel experiments and numerical computations,[17] the flow velocity profile between the train's underbody and the ballast track could be used to calculate the angular impulse exerted on the body (see equation (2)) corresponding to the wind speed at the height h_m from the ballast reference level. The larger the flow speed, the greater the angular impulse on the stone.

Conclusions

The comparative effect of the flow generated on the trackbed by the passage of different trains has been considered in this paper.

The presented analysis is based on a simple theoretical model of the stability limit for stones to begin to roll under the impulses created by the passage of a train. A dimensionless effective gust impulse has been identified as the relevant parameter to be taken into account. It is a function of the geometry of both the body used to measure the pressure loads in on-track tests and of the flow generated under the train, but it does not depend on the ballast properties, ballast posture or surrounding stones. In this way, the train/ballast interaction is split into two parts. The first part, which is studied here, only depends on the aerodynamics and not on the ballast's mass and inertia properties. The second one is the capability of the ballast to resist the mechanical action of the wind, which does depend on the mass and inertia properties, and ballast posture and contacts with other stones.

It is hoped that this separation of the problem can help the relevant rail authorities and standardization organizations to define tests that can identify the effect of trains, independent of the particular ballast on the trackbed. To achieve this end, a standard reference body to measure the gust impact on the ballast is suggested. In this regard, the measurements performed on track tests with a proposed standard reference body show that extreme peaks of aerodynamic loading exist, which can lead to the initiation of motion of the ballast. A single extreme value analysis has been carried out, which has allowed the classification of the tested train models based on the intensity of their corresponding gusts.

On-track experimental results related to the idealization considered in the mathematical model have been presented, and averaged histograms of the dimensionless effective gust impulse for several trains (without giving absolute magnitudes, to preserve confidentiality) have been determined.

Concerning the experimental campaign, the following points should be highlighted.

1. An instrument based on a reference test body has been developed, and its capabilities have been checked on track tests to measure the effect of the aerodynamic load on the ballast produced by the wind gusts generated by the train.
2. The instrument allows for the passing train type to be identified by counting the number of axles, and also determining train speed.
3. The number of passes required to obtain a stable average of the mean value of the several mesurands involved has been determined.
4. A signature for the pressure coefficient versus time, a characteristic of each train, has been identified from the ensemble average of the measurements taken from several train passes. The pattern of this signature appears in all the pressure channels (top of the semi-circular cylinder, cylinder wake, Pitot tube, vertical wall wake).
5. The good agreement between the signals from the redundant twin pressure taps helps to validate this measurement process, which involves noise-like signals.

6. A characteristic curve of the gust-generated impulse as a function of the weight moment coefficient of the ballast can be determined for each train from the impulse histograms obtained. A comparison between the BTE capacities of different trains has been established based on the relative positions of the train-characteristic impulse curves. This is the most relevant result obtained here concerning BTE measurement standardization.
7. The determination, not only in a relative way, but also in an absolute way, of the BTE capability of a given train, it is necessary to evaluate the rolling moment generated by train aerodynamic actions of different types of stones populating the ballast bed surface, (e.g. by experiments in an appropriate wind tunnel).
8. The vertical acceleration at the centre of a sleeper has been measured, and it has been shown that the spectrum is an amalgamation of the track response (high frequency, random response independent of train speed), and the train excitation (low frequency, deterministic range train speed-dependent).
9. In the spectral density, two regions with different types of behaviour have been detected. For a given train, below a frequency of approximately 300 Hz the curves are almost coincident (for a given speed), which suggests the existence of a deterministic range, and above this frequency, the spectral densities show some random contributions, which can be associated with a non-deterministic behaviour.
10. In the deterministic range ($f < 300$ Hz), a dependence of spectral density with train speed has been observed. If the spectrum is plotted using an appropriate dimensionless frequency, the deterministic region can be split into two parts: on the low-frequency side, spectral density decreases with train speed, and on the high-frequency side it increases.

References

Quinn AD, Hayward M, Baker CJ, et al. A full-scale experimental and modelling study of ballast flight under high speed trains. *Proc IMechE, Part F: J Rail Rapid Transit* 2010; 224(2): 61–74.

Morgan RPC. *Soil erosion and conservation*. Oxford, UK: Blackwell Publishing Ltd, 2005.

Sanz-Andres A and Navarro-Medina F. The initiation of motion of a lying object caused by wind gusts. *J Wind Engng Ind Aerodyn* 2010; 98: 772–783.

Kwon HB and Park CS. An experimental study on the relationship between ballast-flying phenomenon and strong wind under high-speed train. In: *The seventh world congress on railway research*, Montreal, Canada, 4–8 June 2006.

Sterling M, Baker CJ, Jordan SC, et al. A study of the slipstreams of high-speed passenger trains and freight trains. *Proc IMechE, Part F: J Rail Rapid Transit* 2008; 222(2): 177–193.

Baker C. The flow around high speed trains. *J Wind Engng Ind Aerodyn* 2010; 98: 277–298.

Owen PR. Saltation of uniform grains in air. *J Fluid Mech* 1964; 20(2): 225–242.

Nalpanis P, Hunt JC and Barret CF. Saltating particles over flat beds. *J Fluid Mech* 1993; 251: 661–685.

Zhang W, Kang JH and Lee SJ. Tracking of saltating sand trajectories over a flat surface embedded in an atmospheric boundary layer. *Geomorphology* 2007; 86: 320–331.

Tropea C, Yarin AL and Foss JF. *Springer handbook of experimental fluid mechanics*. Berlin, Germany: Springer, 2007.

Guckenheimer J and Holmes P. *Nonlinear oscillations, dynamical systems and bifurcations of vector fields*. New York, NY: Springer-Verlag, 1983.

Holmes PJ. The dynamics of repeated impacts with a sinusoidally vibrating table. *J Sound Vib* 1982; 84(2): 173–189.

Wood LA and Byrne KP. Analysis of a random repeated impact process. *J Sound Vib* 1981; 78: 329–345.

Galvin P and Dominguez J. Análisis numérico y experimental de las vibraciones ocasionadas por el paso de trenes de alta velocidad en la línea Córdoba-Málaga. In: *Iberian Latin American Congress on Computational Methods in Engineering*, Porto, Portugal, 13–15 June 2007.

Zhai WM, Wang KY and Lin JH. Modelling and experiment of railway ballast vibrations. *J Sound Vib* 2004; 270: 673–683.

Aydin EM and Leutheusser HJ. Plane-Couette flow between smooth and rough walls. *Exp Fluids* 1991; 11: 302–312.

Garcia J, Crespo A, Berasarte A and Goikoetxea J. Study of the flow between the train underbody and the ballast track. *J Wind Engng Ind Aerodyn* 2011; 99: 1089–1098.

Appendix I

Nomenclature

c_{mge}	weight moment coefficient
c_{p0j}	pressure coefficient at tape j referred to the reference pressure and the train velocity U_T
$c_{p\mathrm{AB}}$	pressure coefficient at A referred to the pressure at B and the train velocity U_T

d	distance between the centre of mass and the pivot point P
f	histogram of one train pass
f_p	averaged histogram
g	acceleration due to gravity
Δh	height increment of the centre of mass
I	moment of inertia with regard to point P
k_a	moment safety factor for unfulfilled assumptions
k_I	ratio of the radius of gyration around point P and the side of the cube
k_s	efficiency factor
l	side of the modelled cubic stone
m_p	mass of the stone
M_{aP}	aerodynamic moment with regard to point P
N_p	number of passes of a train
p	fluid pressure
p_A	pressure at the windward side of the stone model
p_B	pressure at the leeward side of the stone model
r_{gP}	radius of gyration around point P
S_n	dimensionless angular impulse
S_{nx}	singular extreme of the dimensionless angular impulse
s_n	angular impulse
t	time
t_1	time instant when M_{aP} exceeds the gravity moment
t_2	time instant when M_{aP} is again smaller than the gravity moment
t_3	time instant when the centre of mass reaches the maximum height
t_{cn}	characteristic time of the gust
t_{crg}	characteristic time of the stone rotation motion due to gravity
U_r	incoming flow speed
U_T	train speed
x	longitudinal position along the train
θ	angular position of the body
θ_{max}	maximum angular position of the body
ρ_a	density of air

Appendix 2

Detailed description of mathematical model

A simple model has been developed in order to estimate the angular impulse exerted on a standard body by a gust generated by a train. The motion of a cube, with side l, initially lying on the ground, which can rotate around its trailing edge (Figure 1), under the aerodynamic forces produced by the incoming flow $U_r(t)$, generated by a train pass is considered in this paper. Assuming that the pressure is reasonably evenly distributed along the windward side p_A and leeward side p_B, that the pressure on the top is the same as on the leeward side p_B, and in the lower side it is also p_A (the stagnation pressure), the aerodynamic moment with regard to P, M_{aP} is given by

$$M_{aP} = (p_A - p_B) l^3 k_a \tag{10}$$

where k_a is a factor that takes into account the degree that the assumptions are not valid, e.g. pressure uniformity.

The equation of rotational motion around P is given by

$$I\ddot{\theta} = k_a(p_A - p_B) l^3 - m_p g d \cos\theta_{cm} \tag{11}$$

where I is the moment of inertia around an axis which coincides with the cube edge at P, θ the angular position of the body, m_p the body mass, g the acceleration due to gravity, d the distance from the centre of mass to point P and θ_{cm} the angular position of the centre of mass. The motion starts at the time instant $t = t_1$ when the moment M_{aP} exceeds the moment due to gravity

$$\ddot{\theta}(t_1) = 0 \quad \text{with} \quad \ddot{\theta}(t_1) > 0 \tag{12}$$

The pressure jump $p_A - p_B$ is a function of time, as the flow is unsteady. If $p_A - p_B$ is known, e.g. from measurements obtained with the body placed on the track, the time evolution of θ can be obtained by the integration of equation (11), starting at the instant t_1 fulfilling conditions (12).

The angular impulse, s_n, exerted on the body over the time interval from $t = t_1$ to $t = t_2$, is given by

$$\begin{aligned} s_n &= \int_{t_1}^{t_2} \left[k_a(p_A - p_B) l^3 - m_p g d \cos\theta_{cm}\right] dt \\ &\cong \int_{t_1}^{t_2} \left[k_a(p_A - p_B) l^3 - m_p g \frac{l}{2}\right] dt \end{aligned} \tag{13}$$

where it has been assumed that the centre of mass is placed at the centre of the body, and that the angle $\theta_{cm} \approx \pi/4$ remains constant as a consequence of considering short duration gusts.

Also, to ease the calculation, the net torque is neglected from t_2 onwards. t_2 is the time instant when the net moment returns to zero, $\ddot{\theta} = 0$ with $\ddot{\theta} \leqslant 0$. Thus, it is possible to decouple the stone's dynamics from the evolution of the aerodynamic loads due to the stone's motion (which is associated with the change of angle of attack and the rotation speed).

The rotational velocity of the body at the instant $t = t_2$ can be evaluated by integrating equation (11) from $t = t_1$ to $t = t_2$

$$\dot{\theta}(t_2) = \frac{1}{I} s_n \tag{14}$$

Even if the duration of the gust is short, the gust intensity can be large enough to exert an angular impulse such that at $t=t_2$ the angular speed $\dot{\theta}(t_2)$ equals $\dot{\theta}_{\text{crit}}$, which is the speed required for the centre of mass to reach the maximum height, at zero speed, which occurs at $t=t_3$ (Figure 1(c)).

From this time instant, t_3, onwards, the body continues to rotate, the height of the centre of mass decreases, and thus the force of gravity helps the aerodynamic forces to accelerate the rotational motion.

This phase of the motion can be easily analysed by using the principle of conservation of the mechanical energy between $t=t_2$ and $t=t_3$. At $t=t_2$ the height of the centre of mass has its lowest value and $\dot{\theta}(t_2)=\dot{\theta}_{\text{crit}}$, and at $t=t_3$ the height of the centre of mass is at its highest value, at zero speed, $\dot{\theta}(t_3)=0$. Therefore

$$\frac{1}{2}I\dot{\theta}_{\text{crit}}^2 = m_p g \Delta h \tag{15}$$

where Δh is the increment in the height of the centre of mass, and hence

$$\dot{\theta}_{\text{crit}} = \sqrt{\frac{2m_p g\Delta h}{I}} = \sqrt{\frac{2m_p g\Delta h}{m_p r_{gP}^2}} = \sqrt{2\frac{g\Delta h}{k_I^2 l^2}} = \frac{\sqrt{2}}{t_{crg}} \tag{16}$$

where $I=r_{gP}^2 m_p$, and $k_I = r_{gP}/l$, $t_{crg}=k_I l/\sqrt{g\Delta h}$ is the characteristic time associated with the rotational motion around P due to gravity.

The impulse generated by the gust is transformed into angular momentum, or angular kinetic energy, leading to the rotation of the stone around the pivot point P, even if the gust has decreased in intensity. This energy is then transformed into potential gravitational energy.

In the case considered here (a short duration but intense gust) the angular impulse can be determined from the pressure jump $(p_A - p_B)$ measurements taken on a stationary body. To make the results more general, it is appropriate to use the angular impulse defined in equation (13) but written in dimensionless form, S_n, as follows

$$S_n = \frac{s_n}{\rho_a U_T^2 l^3 k_a t_{cn}/2} = \int_{t_1}^{t_2}\left[\frac{p_A - p_B}{\rho_a U_T^2/2} - \frac{m_p g}{\rho_a U_T^2 l^2 k_a/22}\right]\frac{dt}{t_{cn}}$$

$$= \int_{t_1}^{t_2}\left[c_{pAB}(t) - c_{mge}\right]\frac{dt}{t_{cn}}, \tag{17}$$

where $c_{pAB}(t)$ is the pressure coefficient at A referred to the pressure p_B, and made dimensionless with the dynamic pressure related to the train velocity U_T

$$c_{pAB}(t) = \frac{p_A - p_B}{\rho_a U_T^2/2} \tag{18}$$

t_{cn} is a characteristic time of the gust duration, which is arbitrarily taken as $t_{cn}=10^{-2}$ s (which is a typical value). c_{mge} is the coefficient of weight moment with regard to point P, at $t=t_1$ (when the net moment is zero).

From the zero net moment condition at $t=t_1$ (equation (12)) and at $t=t_2$ (the assumed end of the effective impulse application), the condition $c_{pAB}(t_1)=c_{pAB}(t_2)=c_{mge}$ is obtained, where

$$c_{mge} = \frac{m_p g l/2}{\rho_a U_T^2 l^2 k_a/2}. \tag{19}$$

Appendix 3

Reynolds number effects

In a general situation, the pressure coefficient depends on the Reynolds number of the flow $Re=UL/\nu$, until some critical value Re_c is reached, beyond which it remains almost constant. U is the characteristic flow speed, L is the characteristic object longitude and ν is the Kinematic viscosity. In the case of bluff bodies with sharp edges, it is $Re_c \approx 2000$.

In the ballast configuration ($U \approx 10$ m/s, $L \approx 0.03$ m, $\nu = 1.5 \times 10{-}^5$ m^2/s), the Reynolds number is $Re=20{,}000$ that is $Re > Re_c$, and therefore the pressure coefficients obtained for speeds larger than 10 m/s can be considered valid in this range, and therefore independent of velocity.

This result allows the results obtained here, although obtained at some particular train speeds, to be applicable in the whole range of train speeds of interest, say $U_T > 60$ m/s.

Appendix 4

Ballast characteristics

The following results were obtained from measurements performed on small-sized sample ballast taken from the track.

1. The lightest fraction of the sample have masses $m_p < 100$ g, and sizes between $4 \times 3 \times 2$ cm and $5 \times 5 \times 1$ cm (flat stones), with volumes between 18 and 30 cm^3.
2. The intermediate fraction is composed of stones with masses in the range $100 < m_p < 140$ g, and sizes of the order of $4 \times 4 \times 2$ (32 cm^3), which is slightly larger than the size of the lightest fraction.

In this study a stone of mass 140 g and characteristic size $l=3$ cm is considered as a reference, and for the aerodynamic properties the following values of train speed $U_T=80$ m/s and air density $\rho_a=1.2$ kg/m^3 are considered.

From these data the weight moment coefficient $c_{mge}=0.40$ is obtained, and $c_{mge}=0.26$ if $U_T=100$ m/s.